Worldwide assessments of laser radar tactical scenario performance variability for diverse low altitude atmospheric conditions at 1.0642 μm and 1.557 μm

Steven T. Fiorino[a], Richard J. Bartell[a], Matthew J. Krizo[a], Daniel J. Fedyk[a] Kenneth P. Moore[a], Thomas R. Harris[a], Salvatore J. Cusumano[a], Richard Richmond[b], and Matthew J. Gebhardt[b]

[a]Air Force Institute of Technology, Center for Directed Energy, 2950 Hobson Way, Wright-Patterson AFB, OH 45433-7765
steven.fiorino@afit.edu

[b]Air Force Research Laboratory, Sensors Directorate, 3109 Hobson Way, Wright-Patterson AFB, OH 45433-7700
richard.richmond@wpafb.af.mil

Abstract: Spatial, spectral and temporal variations in operating conditions are major contributors to the expected variability/uncertainty in system performance. The ratio of signal-to-noise ratio (SNR) based on climatological data to a standard atmosphere is the primary performance metric used, with results presented in the form of histograms and maps of worldwide LADAR performance variation. This metric is assessed at 2 wavelengths, 1.0642 μm and 1.557 μm, for a number of widely dispersed land and maritime locations worldwide over oblique and vertical air to surface paths in which anticipated clear air aerosols and location specific heavy rain and 150 m thick fog occur. Seasonal, boundary layer, and time of day variations for a range of relative humidity percentiles are also considered. In addition to realistic vertical profiles of molecular and aerosol extinction, air-to-ground cloud free line of sight (CFLOS) probabilities as a function of location for this geometry are computed. Observations from the current study strongly indicate that use of the standard atmosphere to predict performance will produce overly optimistic, in many cases extremely so, estimates of expected performance. Locally heavy rain, when present, severely limits LADAR system performance at these wavelengths. Some operational capability exists for vertical looks through fog.

Keywords: LADAR, cloud free line of sight, atmospheric path extinction, rain rate, fog.

1 INTRODUCTION

Modeling and simulation can make important direct contributions to the joint warfighting community by helping to establish clear and fully integrated future program requirements. These requirements are best determined via analysis of the expected variability/uncertainty in system performance arising from spatial, spectral and temporal variations in operating conditions. In this study, the High Energy Laser End-to-End Operational Simulation (HELEEOS) modeling and simulation tool, in conjunction with a LADAR performance model developed by the Sensors Directorate of the Air Force Research Laboratory, is used to compare the expected signal to noise ratio performance of LADAR systems operating at 1.0642 μm and 1.557 μm for a number of widely dispersed land and maritime locations worldwide to that predicted for a standard atmosphere. The "standard atmosphere" for this

Received 30 Jan 2008; accepted 24 Mar 2009; published 31 Mar 2009 [CCC: 19313195/2009/$25.00]

study is the often used atmospheric definition of midlatitude north summer with MODTRAN rural aerosols, referenced in the paper as the standard atmosphere. Results for the low altitude oblique slant range scenario studied indicate the probability of a cloud free line of sight (CFLOS) is a significant consideration. Locally heavy rain will greatly limit performance while the rain persists.

1.1 Description of the HELEEOS Model

HELEEOS supports dynamic engagements in which the platform, target and up to two optical relays can move vertically and horizontally on any heading in a true 3-D engagement. Engagement geometry is defined in HELEEOS by user specification of slant ranges, altitudes, headings, horizontal and vertical velocities and accelerations. HELEEOS was developed by the AFIT Center for Directed Energy under the sponsorship of the High Energy Laser Joint Technology Office, and its basic features have been previously described [1].

The HELEEOS model enables the evaluation of uncertainty in high energy laser propagation by incorporating probabilistic climatological data on the parameters that drive most major atmospheric effects. Atmospheric parameters investigated, such as temperature, pressure, water vapor content, optical turbulence, and atmospheric particulates, are put into vertical profiles of data for highly specific modeling scenarios. Worldwide seasonal, diurnal, and geographical spatial-temporal variation in these parameters is organized into probability density function (PDF) databases using a variety of recently available resources to include the Extreme and Percentile Environmental Reference Tables (ExPERT) [2] the Master Database for Optical Turbulence Research in Support of the Airborne Laser [3] the Global Aerosol Data Set (GADS) [4], and Air Force Weather Agency numerical weather forecasting data. GADS provides aerosol constituent number densities on a 5° x 5° grid worldwide. ExPERT mapping software allows the HELEEOS operator to choose from specific site or regional upper air data to characterize correlated molecular absorption, aerosol absorption and scattering by percentile. The PDF nature of the HELEEOS atmospheric effects package enables realistic probabilistic outcome analyses which permit an estimation of the confidence in the calculated probability of effect (P_e). HELEEOS users can additionally access, display and export the atmospheric data independent of a high energy laser (HEL) engagement simulation [5]. The integration of the Surface Marine Gridded Climatology database, the Advanced Navy Aerosol Model (ANAM) [6], and the Navy Surface Layer Optical Turbulence (NSLOT) [7] model provides worldwide coverage over all ocean regions on a 1° x 1° grid. Molecular scattering is computed based on Rayleigh theory. Molecular absorption effects are computed for the top 13 absorbing species using line strength information from the HITRAN 2004 database [8] in conjunction with a community standard molecular absorption continuum code. Aerosol and hydrometeor scattering and absorption are computed with the Wiscombe [9] Mie module.

Vertical profiles of molecular absorption and molecular scattering can be defined in a number of ways in HELEEOS. Along with the US Standard Atmosphere 1976, twelve standard atmospheres representing summer and winter conditions for the major climate regions are available (midltitude north summer is used as “standard” for this study). In addition, a large number of specific worldwide surface locations defined in ExPERT, as well as any ocean location on the 1° x 1° latitude/longitude grid, can be selected. The ExPERT and oceanic data allow the lowest, most dense, layers of the atmosphere to be more realistically defined in comparison to the definitions available from the widely used US Standard or regional standard atmospheres.

The red circles in Fig. 1 indicate the 408 ground sites available from ExPERT in HELEEOS. The user can also select from 1 of 9 relative humidity percentile conditions (ranging from 1st to 99th percentiles) to model, with the default being 50th percentile conditions, as well as time of day in 3 hour local time blocks for any of these sites.

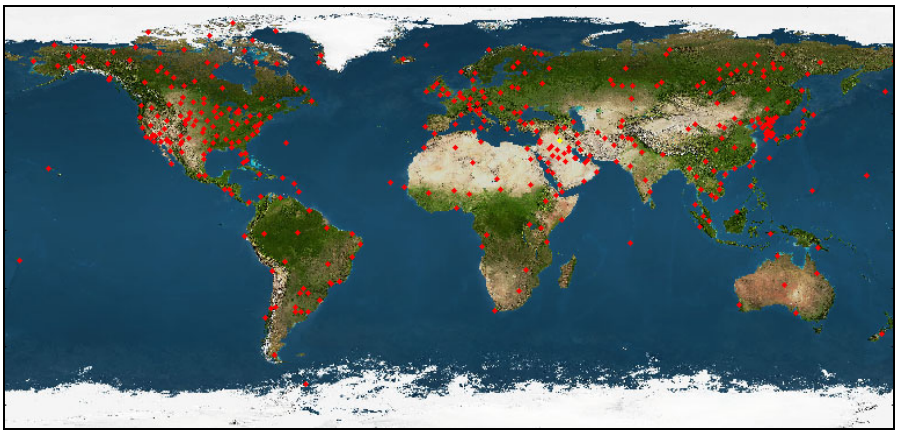

Fig. 1. The 408 worldwide land locations represented in HELEEOS.

A diverse array of aerosol vertical profiles is also available. There are 10 profiles defined using the Optical Properties of Aerosols and Clouds (OPAC) [10] code, 3 MODTRAN aerosol profiles [11], and the windspeed-driven aerosol mixtures from ANAM. The aerosol profile for each ExPERT site is defined using the constituent data from GADS. The GADS aerosol climatologies coupled with the associated OPAC refractive indices are currently considered the community standard. ANAM is considered the standard over the ocean. The MODTRAN aerosol definitions are a legacy from the earliest aerosol optical properties characterizations. Favorable comparisons of GADS/OPAC-derived extinction values to actual vertical profiles of aerosol extinction can be found in [12].

HELEEOS allows the definition of 5 liquid water cloud types, 3 ice (cirrus) cloud types, water fog, ice fog, 5 rain rates and a drizzle characterization. The liquid water and ice clouds and fog are characterized using OPAC distributions, while the rain cases (with the exception of drizzle) are defined using a Marshall-Palmer [13] distribution.

Several optical turbulence profiles are available in the model, for example, Hufnagel-Valley 5/7 [14] and Clear 1 [15]. The climatological C_n^2 profile is a novel feature of HELEEOS. It combines the extensive climatological record of the ExPERT database with the optical turbulence data of the Master Database for Optical Turbulence Research in Support of the Airborne Laser. The optical turbulence database is a direct compilation of many worldwide nighttime thermosonde campaigns. Each climatological C_n^2 profile is tailored to individual sites by distinctly referencing the optical turbulence database based on user-selected surface relative humidities. HELEEOS physically correlates temperature and relative humidity percentiles to corresponding percentage values in the optical turbulence database. Within the boundary layer, HELEEOS correlates the optical turbulence profiles to percentiles of relative humidity, and in the free atmosphere to standard atmosphere temperatures percentiles. These physical correlations to probabilistic climatology form the basis of the climatological C_n^2 profiles, a feature unique to the HELEEOS engagement package [16]. Over the first 50 m of the ocean surface, HELEEOS employs the NSLOT model. Above the lowest 50 m, the Hufnagel-Valley 5/7 model is used to define over-ocean C_n^2 values.

CFLOS probability is incorporated into HELEEOS for air-to-air, air-to-ground, and ground-to-air (or space) look angles at most of the 400+ ExPERT land sites. The air-to-air and air-to-ground CFLOS probabilities are obtained via an integration of Air Force Combat Climatology Center (AFCCC) ground-to-space CFLOS tables with AFCCC ceiling height data [17].

HELEEOS supports any user-defined wavelength from 0.40 μm to 8.6 m, with 24 wavelengths associated with laser operation available via lookup table for minimum runtime.

2 METHODOLOGY

In previous analyses, HELEEOS has been used to analyze various aspects of worldwide high energy laser performance based on the climatological model [18]. In the current study, the capabilities of the HELEEOS model are exploited for the first time to study the worldwide variance in low altitude LADAR system performance across a broad range of atmospheric conditions, including the effects of locally heavy rain. Parameters varied as part of the study:

- 2 wavelengths:
  - 1.0642, 1.557 μm
- 408 ExPERT surface locations worldwide; shown in Fig. 1
- Oceanic locations on a 1° x 1° latitude/longitude grid, approximately 44000
- Atmospheric conditions:
  - 10th, 50th, 90th percentile relative humidity conditions
  - 0300-0600 L, 1500-1800 L and daily average for all land sites
  - variable boundary layer height, dependent upon time of day, location, and season (for land sites)
  - Summer and winter seasons
  - Clear sky aerosols exhibiting geographic and seasonal variation
  - Heavy rain, with rate set as a function of location
  - 150 m thick fog layer
- Geometry:
  - Air-to-Surface, 1530 m and 3000 m slant range
  - Platform (laser) altitude 1525 meters
  - Target altitude 0 meters.

2.1 LADAR System Signal to Noise Ratio

In the current study the impact of variations in atmospheric path transmittance on the signal to noise ratio performance of a hypothetical LADAR is assessed. The first step in computing signal to noise ratio is establishing the noise equivalent power (NEP) of this system. Here NEP is defined:

$$NEP = \frac{hc}{\lambda} \cdot \frac{2B}{\eta} \tag{1}$$

where h is Planck's constant, c is the speed of light, λ is the LADAR wavelength, B is the bandwidth, and η is the quantum efficiency. Next, the standard laser radar equation for extended Lambertian targets is applied [19]:

$$P_r = P_s \cdot \frac{D^2}{4R^2} \cdot \rho \cdot T \cdot \eta_t \cdot \eta_r \tag{2}$$

where P_r is the power received, P_s is the power transmitted, D is the aperture diameter (assumed 80 mm), R is the slant range, ρ is the optimal reflectivity of 33.33% for targets, T is the roundtrip atmospheric path transmittance, η_t is the nominal system optics efficiency (here assumed 0.80), and η_r is the nominal receiver optical efficiency, (here assumed 0.80). Finally, signal to noise ratio is computed as the ratio of P_r to NEP.

3 RESULTS

Variations in atmospheric path transmittance were computed initially and used with the laser radar equation to determine the effect on system SNR.

3.1 Climatology Based Transmittance vs Standard Atmosphere Transmittance

Considering first the ExPERT land sites over the low-altitude short slant range condition of this study, climatalogically-based transmittance for 50th percentile relative humidity, daily average conditions, is similar to that of the standard atmosphere for many locations. This is illustrated for summer conditions at 1.557 μm in Fig. 2. Climatalogically-based values are slightly lower for summer conditions in regions such as eastern North America, Europe and East Asia. In winter, conditions are somewhat improved in eastern Asia due to the influence of Siberian high pressure, but considerably worse in the Middle East, Europe and eastern North America.

A number of observations may be made regarding conditions shown in Fig. 2 over the ocean regions. At high northern and southern latitudes in both summer and winter, climatological data indicates transmittance values significantly lower than that of the standard atmosphere due to a combination of high relative humidity (RH) and wind speed conditions. Higher wind speeds over ocean areas generate more sea salt aerosols; these aerosols are hygroscopic and tend to become larger as RH approaches 100%. High wind speeds and high RHs combine to create larger aerosol concentrations and size distributions over the high ocean latitudes. In the ocean midlatitudes, climatalogically-based transmittance is more similar to that for the standard atmosphere, but still 10% to 30% lower in general.

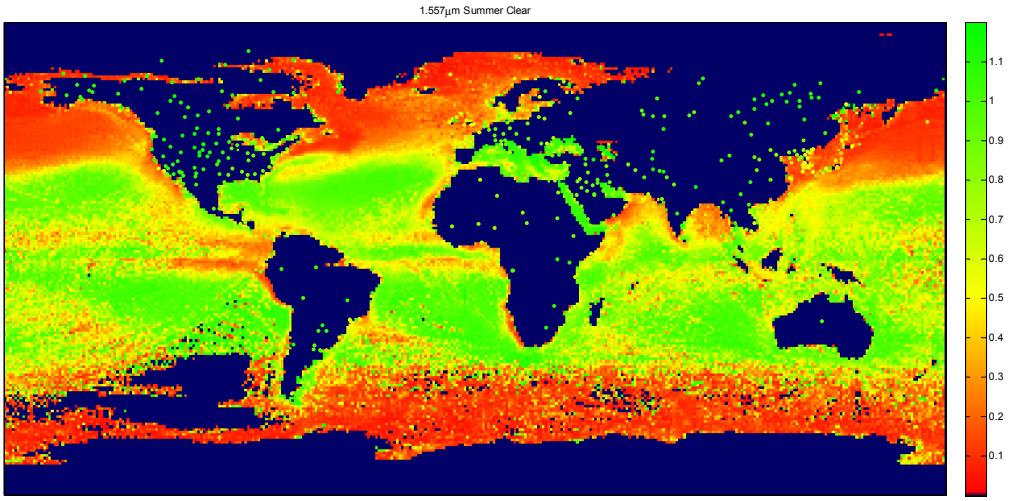

Fig. 2. Worldwide ratios of transmission values for the climatological atmosphere to the standard atmosphere for 1.557 μm, summer, 50th percentile RH, daily average, aerosols only, 3 km slant range.

Path transmittance at 1.557 μm tracks well with that at 1.0642 μm, but because it is a slightly longer wavelength, is less affected by aerosol extinction and path transmittance is approximately 10% greater. Given these similarities, this study concentrates on 1.0642 μm results.

Figure 3 compares total atmospheric extinction, due to the combined effects of molecular scattering, molecular absorption, aerosol scattering, and aerosol absorption, as a function of altitude between the surface and 1600 m for the standard atmosphere to climatologically-based profiles for 4 geographically diverse ExPERT locations, for summer and winter

conditions at 1.0642 μm, 50th percentile RH, 1500-1800 local time conditions. All four sites and the standard atmosphere exhibit greater extinction in the boundary layer (BL) due to the effects of aerosols mixed throughout the BL, which extends to a depth of ~1525 m at 1500-1800 L. Several observations can be made about the ExPERT (climatological) locations: all 4 sites show extinction increasing with height in the BL, or greater extinction than standard, or both. The North Korean site is the most stressing (greatest extinction) of the 4 locations, in both summer and winter. The North Korea, Panama, and Romania locations clearly depict the effects of water soluble aerosols as aerosol extinction—primarily due to scattering—increases dramatically with increasing RH in the well-mixed BL. The extinction traces at these three sites reach a maximum when the RH reaches 100%. Relative humidity increases with height in a well-mixed boundary layer due to temperature lapsing (decreasing) with height while water vapor mixing ratio remains nearly constant. In the Baghdad case, aerosol scattering does not spike with height in the BL during summer; this is because RH throughout the BL is very low in the summer and desert aerosols (like those found in Iraq) are not nearly as water absorbing as those found over much of the earth's land and ocean areas. In winter, the Baghdad extinction does increase with height because cooler temperatures create higher RHs which allow for the water soluble-components mixed with the desert aerosols to grow in size with height.

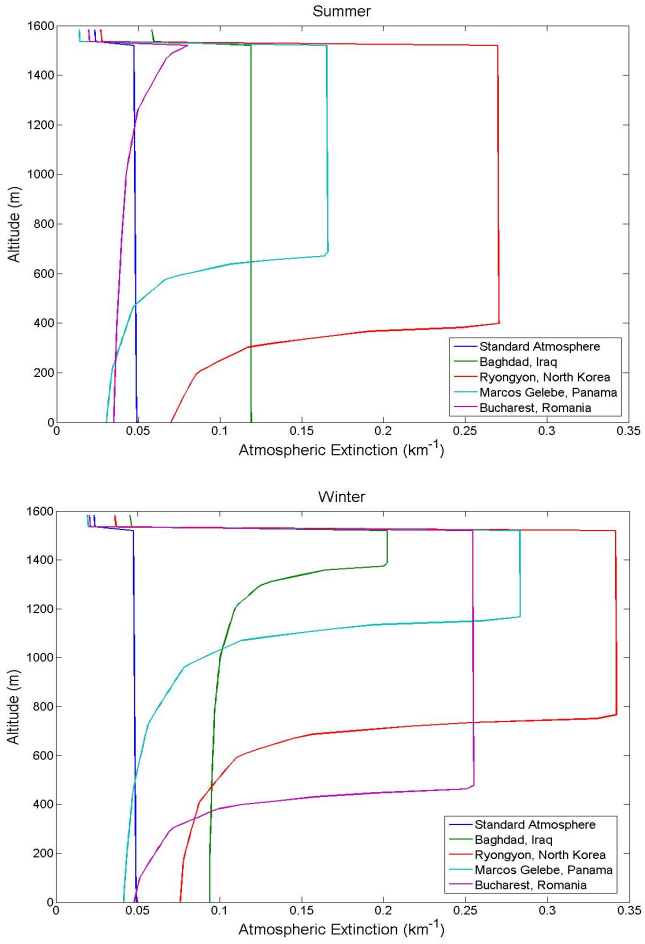

Fig. 3. Vertical profiles of extinction for 1.0642 μm, summer (Top) and winter (Bottom), 1500-1800L, for 4 diverse ExPERT locations vs. standard atmosphere.

Note that in almost all the climatological cases shown in Fig. 3, the extinction due to the boundary layer is significantly greater than standard. The exception is the Romanian site in summer; this is because the standard atmosphere is based on an average midlatitude north summer atmosphere with rural aerosols—Bucharest, Romania is climatologically a good example of a midlatitude north site.

3.2 Probability of Cloud Free Line of Sight

A key consideration for electro-optical and infrared systems is the probability of cloud free line of sight between the platform and target.

In Fig. 4 we see that for the relatively short, low altitude oblique 3000 m slant range scenario for summer conditions, 1500-1800 local time, there are many locations, particularly in the tropics, where the probability of cloud free line of sight is on the order of 50%. This is a potentially significant operating constraint. In the early morning, winter case (bottom chart of Fig. 4), CFLOS probability remains reduced in northwestern and central Europe relative to other regions, despite this time of day typically having less low-level cloudiness. Increasing the platform altitude will decrease, in some locations markedly, the CFLOS probability.

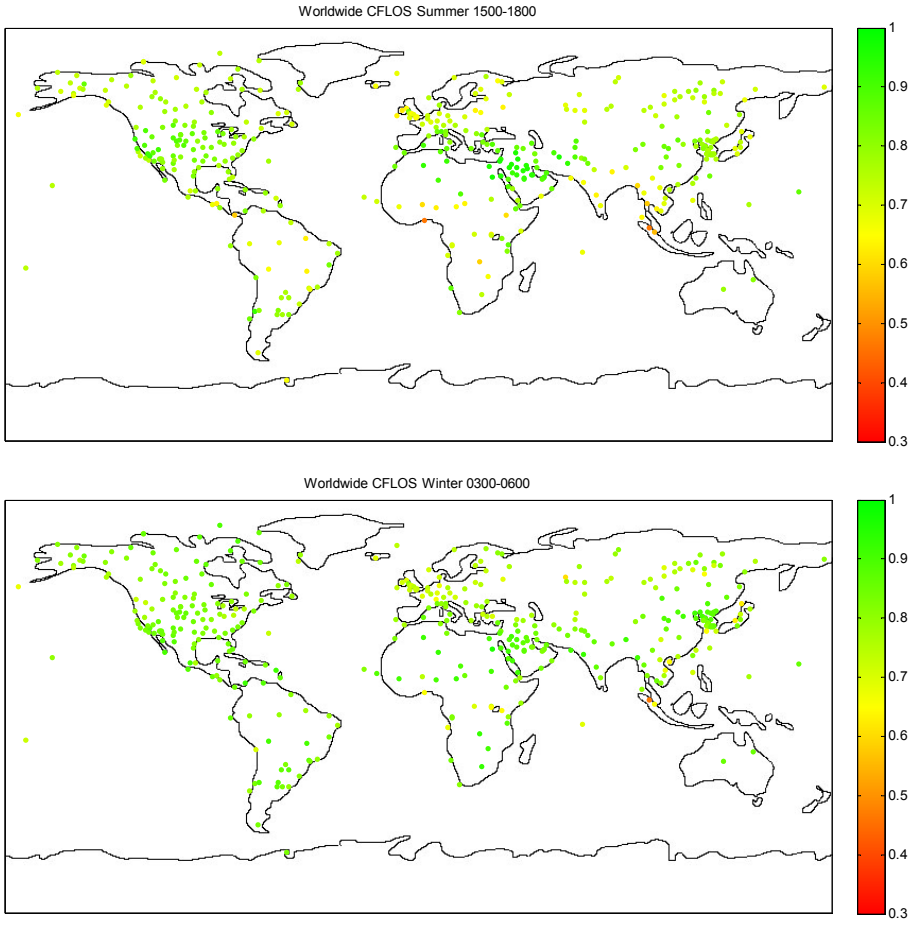

Fig. 4. Probability of cloud free line of sight for the geometry used in the study, summer, 1500-1800 local time (Top) and winter, 0300-0600 local time (Bottom).

3.3 Signal to Noise Ratio Comparison Results

Figure 5 depicts composite worldwide SNR metric results for all 408 ExPERT land locations and all available oceanic locations at 1.0642 μm, daily average (all times), 50th percentile relative humidity conditions, for summer and winter respectively, for the 3000 m slant range case. These land/ocean composite comparisons can only be made for 50th percentile relative humidity conditions because only 50th percentile data are currently available for ocean locations. The SNR metric results are highly correlated with path transmittance variations. Climatologically-based SNR metric values are lower for summer conditions in regions such as eastern North America, Europe and East Asia. In winter, conditions improve in eastern Asia due to the influence of Siberian high pressure, but are considerably worse in the Middle East, Europe and eastern North America, due to higher winter relative humidity. At northern and southern latitudes over the oceans, for both summer and winter, climatologically based SNR metric values are significantly lower than that of the standard atmosphere due to a combination of high wind speed and RH conditions.

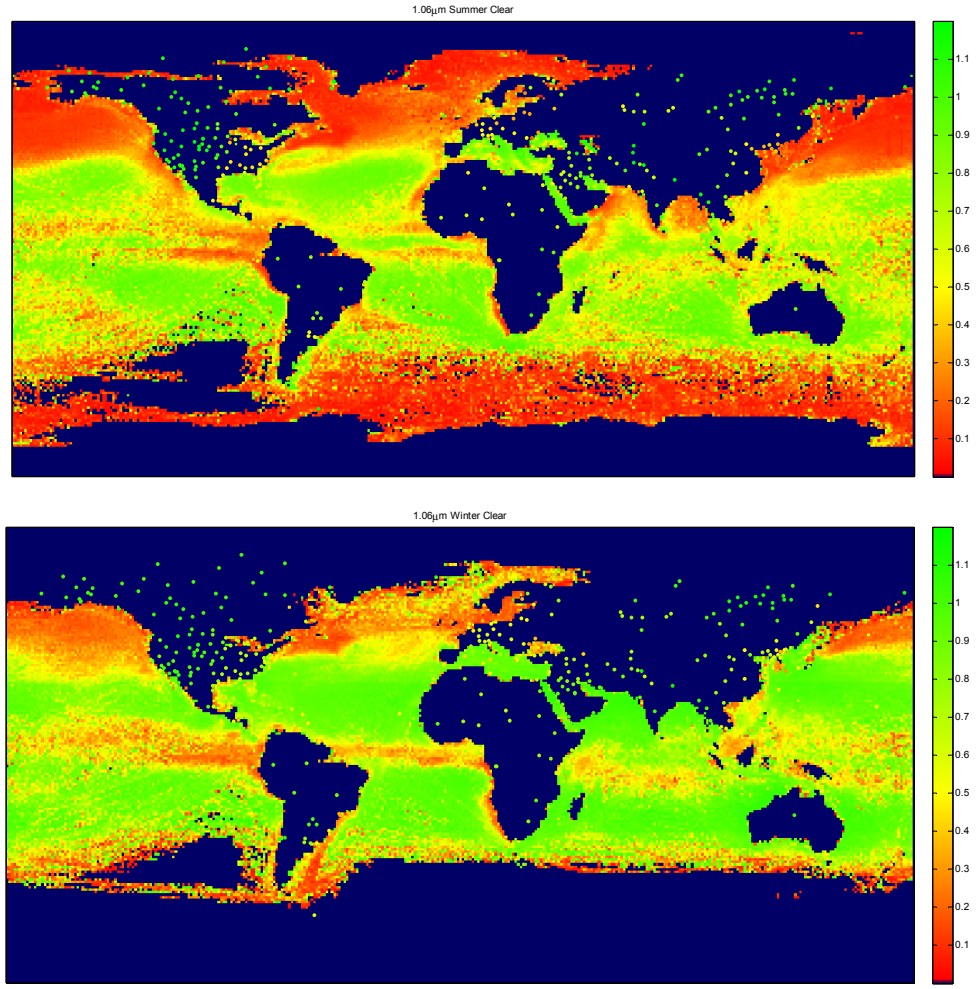

Fig. 5. Worldwide ratios of SNR values for climatological atmosphere to standard atmosphere for 1.0642 μm, for summer (Top) and winter (Bottom), 50th percentile RH, daily average, aerosols only, 3000 m slant range.

Figure 6 contains histograms of these worldwide, 50th RH percentile, daily average results for the 3000 m slant range case. Climatological conditions for the ocean regions are less favorable overall vis-à-vis the standard atmosphere than those for the land sites. One of the most significant differences between the ocean and land scenarios in Fig. 6 is nearly 25% of the 408 modeled land engagements exhibit better SNR for the climatological atmospheres; the standard atmosphere SNR is more favorable over the ocean in virtually 100% of the scenarios modeled there.

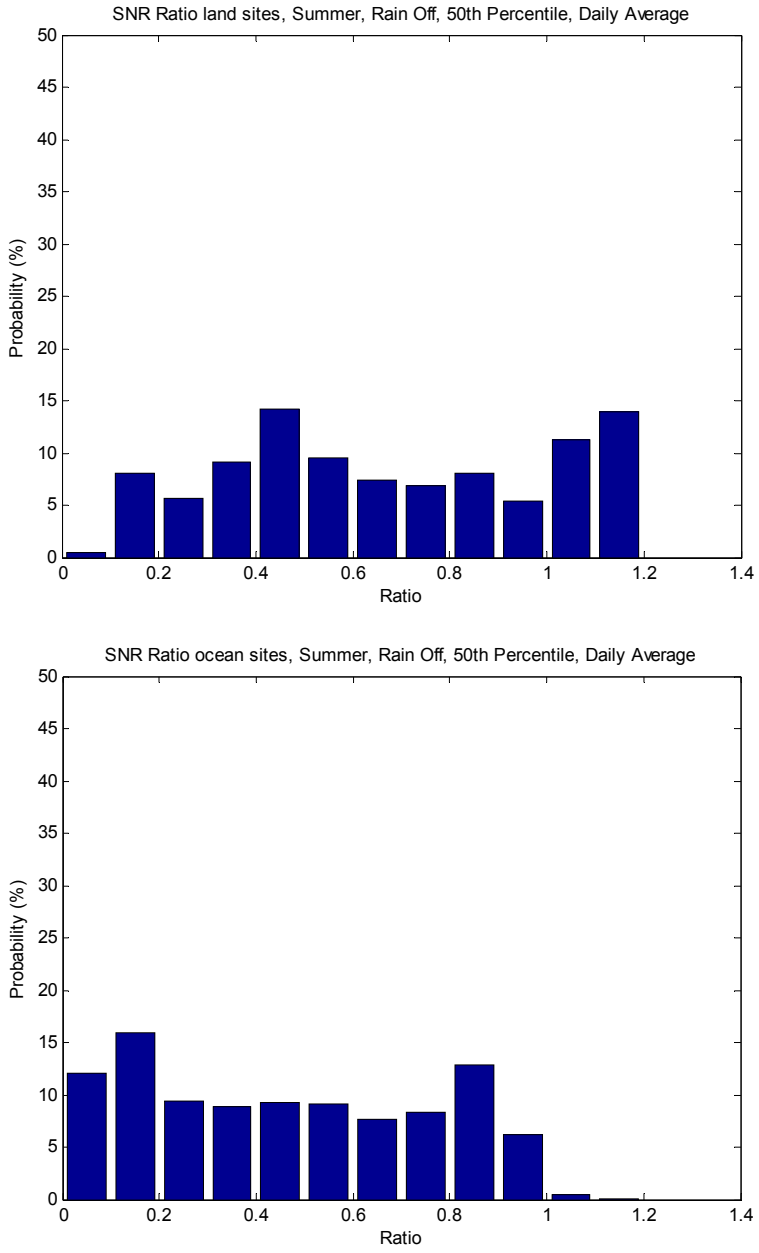

Fig. 6. Histogram of worldwide ratios of SNR values for climatological atmosphere to standard atmosphere for 1.0642 μm, summer, daily average, land sites (Top), ocean sites (Bottom), 3000 m slant range case.

Figure 7 graphically illustrates the variation in performance across the geographic, time of day, and seasonal dimensions of the climatological database available the 408 ExPERT sites, again for the 3000 m slant range case. The 10th percentile RH conditions in the late afternoon summer are typically associated with the smallest aerosol size distributions. The 90th percentile, early morning winter conditions are usually associated with the largest aerosol size distributions. As can be seen in Fig. 7, the 90th percentile relative humidity, winter conditions are significantly more limiting in many locations.

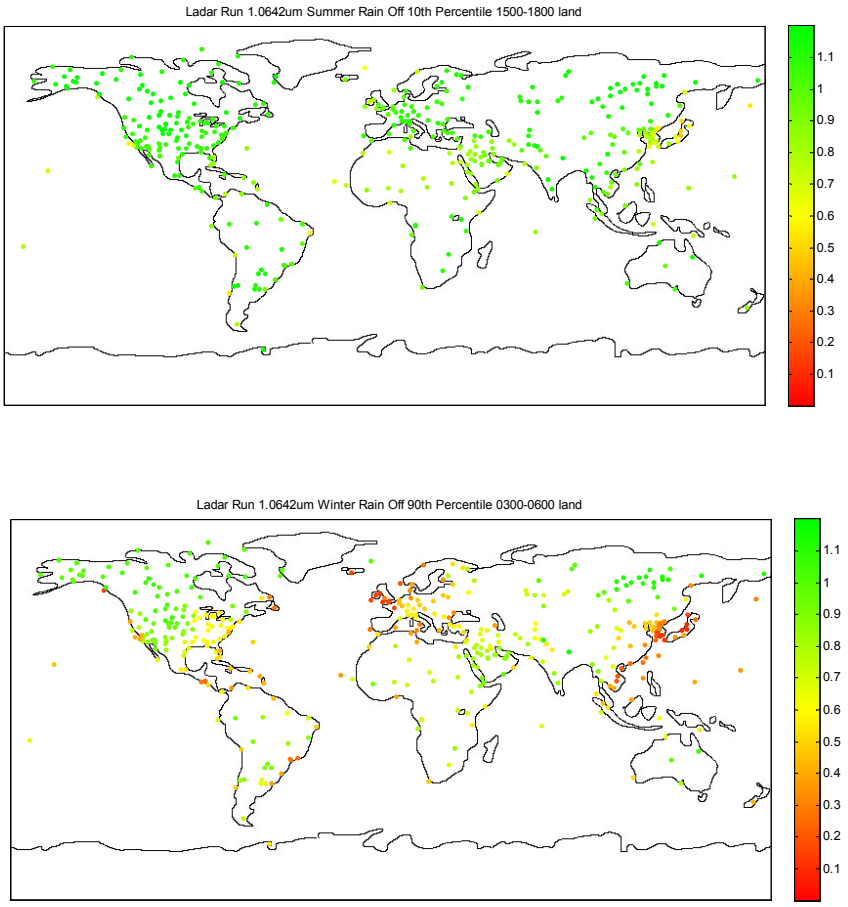

Fig. 7. Comparison of SNR metric results for 10th percentile RH summer, 1500-1800L (Top) and 90th percentile RH winter, 0300-0600L (Bottom) for 1.0642 μm, 3000 m slant range.

Figure 8 is a histogram summary of results for all land sites, summer and winter, all times of day, and all relative humidity conditions. Comparing Fig. 8 to the top plot in Fig. 6, which presents only daily average, 50th percentile RH results in summer, a distinct shift to more extreme scenarios in noted in this global, all-season summary. There is a shift toward very low climatological SNRs due to the 90th percentile RH conditions, and a shift to the highest climatological SNRs as a result of the 10th percentile RH conditions. Overall, the standard atmosphere produced less favorable SNRs in about 25% of the cases, similar to Fig. 6.

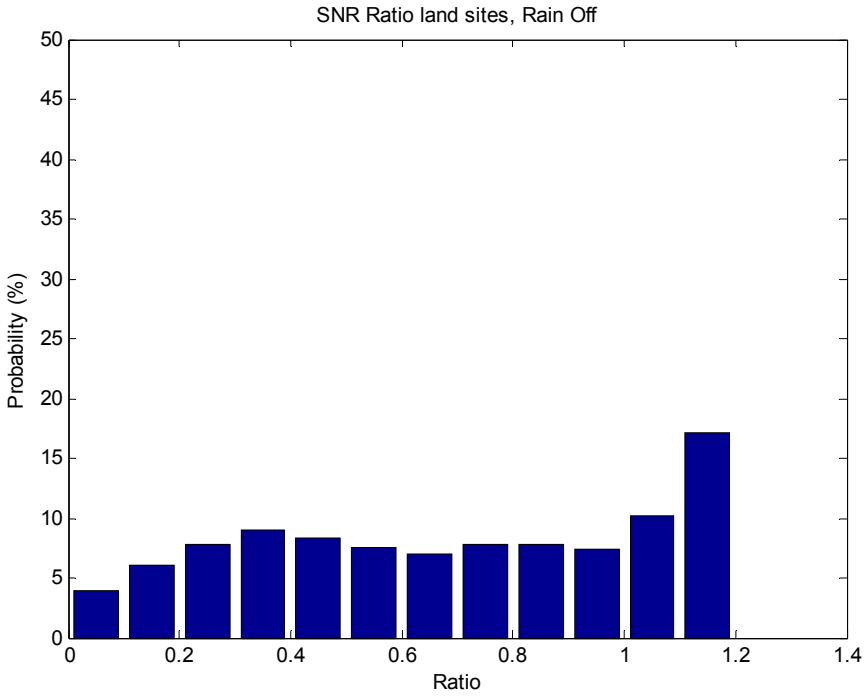

Fig. 8. Histogram results for all times of day, both seasons, all RH percentile conditions, for 1.0642 μm, for 408 ExPERT sites, 3000 m slant range.

3.4 Effects of Location-Dependent Heavy Rain

HELEEOS includes a tool for summarizing probability of rain rate as a function of location, as well as the capability to predict the effect of any specific rain rate on path extinction for any wavelength. The rain rate climatology used in HELEEOS follows that of Crane and Blood [20].

Figure 9 depicts 99.98th percentile rain rates, in mm h^{-1}, for the 408 ExPERT sites, corresponding to locally heavy rain. There is significant variation worldwide, with the heaviest rain rates expected in the tropical regions. These are tabulated on a yearly basis, in most locations these rates correspond to summer conditions. Thus, the 99.98th percentile corresponds to 0.02 percent of the year, or about 1.75 hours per year total. The 0.02 percent threshold was chosen because it is in the middle of the range of "percent of year" values computed for the original Crane and Blood study. The minimum heavy rain rate at the 99.98th percentile level is 12 mm h^{-1} and the maximum is 115 mm h^{-1}.

As one might expect for a LADAR system operating at 1 to 2 μm wavelength, SNR values are dismally low in heavy rain rate scenarios. This is quite apparent in Fig. 10 where the most favorable climatological conditions are coupled with 99.98th percentile rain and then compared via ratio with the standard atmosphere with no rain—the highest ratio is only 0.007. However, such extreme rain rate events occur only 0.02 percent of the year.

3.5 Effects of a 150 m Fog Layer

HELEEOS can also be used to model the effects of water and ice fog, drizzle, and various cloud types in addition to rain, on path transmittance. A 150 m thick water fog layer reduces

SNR to approximately 7% that of the standard atmosphere case for the 3000 m slant range oblique geometry for both wavelengths. 1.0642 μm very slightly outperforms 1.557 μm in the presence of fog. For the nearly vertical 1530 m slant range geometry, the 150 m fog layer reduced SNR to approximately 25% of that for the standard atmosphere condition.

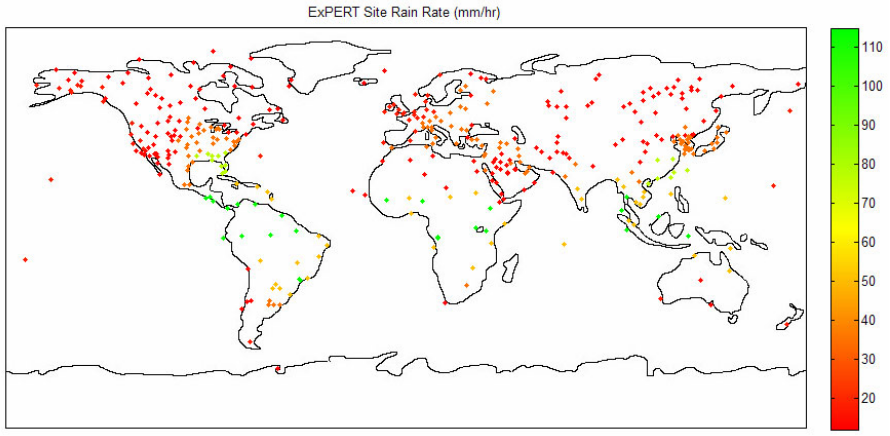

Fig. 9. 99.98th percentile rain rate (mm h-1) for 408 ExPERT sites worldwide.

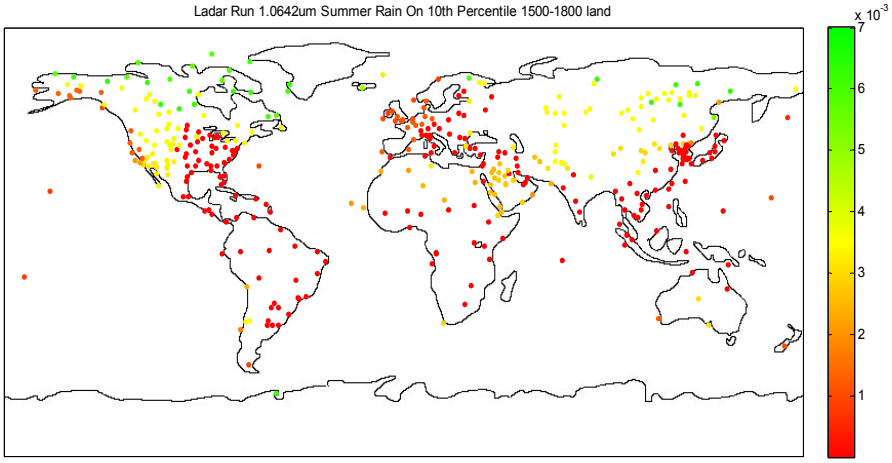

Fig.10. SNR ratio metric at the 408 ExPERT sites worldwide in the presence of locally heavy rain, 3000 m slant range.

4 SUMMARY

Effects of using geographic location, time of day, season, and relative humidity percentile-specific climatological data in lieu of a standard atmosphere in determination of LADAR SNR have been analyzed. In the absence of clouds and precipitation, aerosols are the primary attenuator of 1 to 2 μm LADAR SNR performance in scenarios traversing the atmospheric boundary layer. These aerosols are in general modified by relative humidity, thus causing boundary layer SNR to be highly sensitive to time of day and year. Climatological conditions over the oceans are less favorable in general than those prevailing at land sites vis-à-vis the standard atmosphere. For approximately 75% of the over land condition combinations analyzed, the SNR metric computed for climatological data was less than 1. Nearly all ocean locations were less than 1. These observations strongly indicate that use of the standard

atmosphere to predict performance will produce overly optimistic, in many cases extremely so, estimates of expected performance for the vast majority of location/time of day/season/RH percentile realizations. In addition, the current study indicates that even for the relatively low altitude, short slant range geometry analyzed, cloud free line of sight will be an issue in many locations, particularly in tropical summer conditions and in northwestern and central Europe in winter conditions.

Locally heavy rain will severely limit LADAR system performance at these wavelengths during the periods of time such rain fall persists. The simulations also suggest there exists some operational capability for near-vertical slant paths through fog depths up to 150 m.

Acknowledgments

The authors recognize the outstanding support of the High Energy Laser Joint Technology Office, Albuquerque, New Mexico. The views expressed in this paper are those of the authors and do not necessarily reflect the official policy or position of the Air Force, the Department of Defense or the U.S. Government.

References

[1] R. J. Bartell, G. P. Perram, S. T. Fiorino, S. N. Long, M. J. Houle, C. A. Rice, Z. P. Manning, M. J. Krizo, D. W. Bunch, and L. E. Gravley, "Methodology for comparing worldwide performance of diverse weight-constrained high energy laser systems," *Proc. SPIE* **5792**, 76-87 (2005) [doi:10.1117/12.603384].

[2] M. F. Squires, B. A. Bietler, S.T . Fiorino, D. L. Parks, F. W. Youkhana, and H. D. Smith, "A method for creating regional and worldwide datasets of extreme and average values," *Proc. Inst. Environ. Sci. Annu. Meet*., pp. 6-11 (1995).

[3] A. J. Bussey, J. R. Roadcap, R. R. Beland, and G. Y. Jumper, "Master data base for optical turbulence research in support of airborne laser," *U.S. Air Force Res. Lab. Tech. Rep*. **AFRL-VS-TR-2000-1545** (2000).

[4] P. Koepke, M. Hess, I. Schult, and E.P Shettle, "Global aerosol data set," *MPI Meteorologie Hamburg Rep*. **243**, 44 pp. (1997).

[5] S. T. Fiorino, R. J. Bartell, G. P. Perram, D. W. Bunch, L. E. Gravley, C. A. Rice, Z. P. Manning, and M. J. Krizo, "The HELEEOS atmospheric effects package: a probabilistic method for evaluating uncertainty in low-altitude high energy laser effectiveness," *J. Dir Energy* **1**(4), 347-360 (2006).

[6] S. G. Gathman, A. M. J. van Eijk, and L. H. Cohen, "Characterizing large aerosols in the lowest levels of the marine atmosphere," *Proc. SPIE* **3433**, 41-52 (1998) [doi:10.1117/12.330235].

[7] P. A. Frederickson, K. L. Davidson, C. R. Zeisse, and C. S. Bendall, "Estimates of the refractive index structure parameter (Cn2) over the ocean using bulk methods," *J. Appl. Meterol.* **39**, 1770 (2000).

[8] L. S. Rothman., C. P. Rinsland, A. Goldman, S. T. Massie, D. P Edwards, J. M. Flaud, A. Perrin, C. Camy-Peyret, V. Dana, J. Y. Mandin, J. Schroeder, A. McCann, R. R. Gamanche, R. B. Wattson, K. Yoshino, K. V. Chance, K. W. Jucks, L. R. Brown, V. Nemtchinov, and P. Varanasi, *The HITRAN Molecular Spectroscopic Database and HAWKS (Hitran Atmospheric Workstation)* 2004 ed. (2004).

[9] W. J. Wiscombe, "Improved Mie scattering algorithms," *Appl. Opt*. **19**(9), 1505-1510 (1980 [doi:10.1364/AO.19.001505].

[10] M. Hess, P. Koepke, and I. Schult, "Optical properties of aerosols and clouds: the software package OPAC," *Bull. Am. Met. Soc*. **79**, 831–844 (1998) [doi:10.1175/1520-0477(1998)079<0831:OPOAAC>2.0.CO;2].

[11] E. P. Shettle and R. W. Fenn, "Models for the aerosols of the lower atmosphere and the effects of humidity variations on their optical properties," *Air Force Geophys. Lab. Tech. Rep.* **AFGL-TR-79-0214** (1979).
[12] S. T. Fiorino, R. J. Bartell, M. J. Krizo, G. L. Caylor, K. P. Moore, and S. J. Cusumano, "Validation of a worldwide physics-based high-spectral resolution atmospheric characterization and propagation package for UV to RF wavelengths," *Proc. SPIE* **7090**, 70900I (2008) [doi:10.1117/12.795435].
[13] J. S. Marshall and W. McK. Palmer, "The distribution of raindrops with size," *J. Meterol.* **5**, 165-166 (1948).
[14] R. E. Hufnagel, "Propagation through atmospheric turbulence" *The Infrared Handbook*, W. L. Wolfe and G. J. Zissis, Eds., Infrared Information Analysis Center, Ann Arbor, MI (1985).
[15] R. R. Beland, "Propagation through atmospheric optical turbulence," in *Atmospheric Propagation of Radiation*, pp. 157-232, F.G. Smith, Ed., The Infrared and Electro-Optical Systems Handbook, Vol. **2**, SPIE Press, Bellingham, WA (1993).
[16] L. E. Gravley, S. T. Fiorino, R. J. Bartell, G. P. Perram, M. J. Krizo, and K. Le, "Comparison of climatological optical turbulence profiles to standard, statistical, and numerical models using HELEEOS," *J. Dir. Energy* **3**(1), 347-362 (2007).
[17] S. T. Fiorino, R. J. Bartell, J. D. Eckel, M. J. Krizo, and S. J. Cusumano, "Application and impacts of ground-to-space cloud free line of sight probabilities to air-to-ground high energy laser engagement scenarios," *Proc. 9th Ann. Directed Energy Symp*., Albuquerque, NM (2006).
[18] S. T. Fiorino, R. J. Bartell, G. P. Perram, M. J. Krizo, D. J. Fedyk, B. W. Wisdom, and S. J. Cusumano, "Worldwide estimates and uncertainty assessments of laser propagation for diverse geometries for paths in the altitude regime of 3 km and below at wavelengths of 0.355 μm to 10.6 μm," *Proc. SPIE* **6551** 655104 **(**2007) [doi:10.1117/12.718404].
[19] G.W . Kamerman, "Laser radar," in *Active Electro-Optical Systems*, pp. 1-76, C.S. Fox, Ed., The Infrared and Electro-Optical Systems Handbook, Vol. **6**, SPIE Press, Bellingham, WA (1993).
[20] R. K. Crane and D. W. Blood, "Handbook for the estimation of microwave propagation effects—link calculations for earth-space paths," *Tech. Report* **P-7376-TR1**, 80 pp., Environmental Research and Technology, Inc, Concord, MA (1979).

Steven T. Fiorino, Lt Col, USAF, is an Assistant Professor of Atmospheric Physics at the Air Force Institute of Technology (AFIT). He has B.S. degrees in Geography and Meteorology from Ohio State (1987) and Florida State (1989) universities. He additionally holds an M.S. in Atmospheric Dynamics from Ohio State (1993) and a Ph.D. in Physical Meteorology from Florida State (2002). His research interests include microwave remote sensing, development of weather signal processing algorithms, and atmospheric effects on military systems such as high-energy lasers and weapons of mass destruction.

Richard J. Bartell received his B.S. degree in Physics from the U.S. Air Force Academy as a distinguished graduate in 1979. He received his M.S. degree from the Optical Sciences Center, University of Arizona, in 1987. He is currently a Research Physicist with the Center for Directed Energy of the Air Force Institute of Technology, where he leads development of the High Energy Laser End-to-End Operational Simulation (HELEEOS) model. He is a member of SPIE.

Matthew J. Krizo received his B.S.E.E. from Cedarville University in 2005. He is currently a Research Engineer with the Center for Directed Energy at the Air Force Institute of Technology, Wright Patterson AFB, Ohio. He is primarily responsible for software development of HELEEOS. He is working on a M.S. at the University of Dayton.

Daniel J. Feydk was a student research assistant with the Center for Directed Energy when this work was performed. He completed his M.S.E.E. from the University of Dayton in 2007.

Kenneth P. Moore was a student research assistant with the Center for Directed Energy. He graduated from Cedarville University in 2007 with a B.S. Physics.

Thomas R. Harris was a student research assistant with the Center for Directed Energy. He graduated from Cedarville University in 2008 with a B.S. Physics.

Salvatore J. Cusumano is the Director of the Center for Directed Energy located at AFIT. He received his Ph.D. in Control Theory from the University of Illinois in 1988, a Masters in EE from AFIT in 1977, and a Bachelor in EE from the Air Force Academy in 1971. The Center collaborates on directed energy research topics, both high power microwaves (HPM) and high energy lasers (HEL), throughout the DoD community. Dr. Cusumano's research interests span his 25 years of experience in directed energy and include resonator alignment and stabilization, Intra-Cavity Adaptive Optics, Phased Arrays, telescope control, pointing and tracking, adaptive optics and component technology for directed energy. He holds two patents (jointly) for his work in Phased Arrays.

Richard Richmond works in the Electro-Optics Technology Division of the Air Force Research Laboratory. He is the Team Leader for Laser Radar Technology in the Multi-function Electro-optics Branch. Mr. Richmond has been the Project Engineer or Program Manager on numerous laser radar development and research efforts. Application areas of the various efforts have included both ground-based and airborne wind sensing, imaging and vibration sensing of hard targets, and remote chemical sensing.

Matthew J. Gebhardt received his B.S. Degree in Electrical Engineering from the U.S. Air Force Academy in 1995. He received his M.S. degree in Computer Engineering from the Air Force Institute of Technology in 2000. He is currently the lead technical engineer for the AFRL/RYJM CRAOS (Computational Research for Active Optical Sensors) team where RYJM is developing an advanced ladar computational research environment for ladar predictive modeling, advanced sensor data management, streamlined experiment planning, and advanced algorithm development.